Nanoparticle-Induced Apoptosis Propagates through Hydrogen-Peroxide-Mediated Bystander Killing: Insights from a Human Intestinal Epithelium *In Vitro* Model

Anupama Thubagere and Björn M. Reinhard*

Department of Chemistry and The Photonics Center, Boston University, Boston, Massachusetts 02215

ABSTRACT The ability to assess the risks of human exposure to engineered nanomaterials requires fundamental understanding of the fate and potential cytotoxicity of nonbiodegradable nanoparticles, for instance, after oral uptake. In this study, we quantify the impact of nanoparticles with low chemical toxicity on the intestinal membrane in a human intestinal *in vitro* model. Differentiated human colorectal adenocarcinoma cells, Caco-2, were cultured on a permeable support where they form an epithelial monolayer separating an apical and basal compartment. This model system allows a systematic characterization of the effect of nanoparticles on the cell viability as a function of size, surface chemistry, concentration, and incubation time. We used polystyrene (PS) nanoparticles (20 and 40 nm diameter) with two different surface chemistries (carboxylic acid and amines). The experiments performed show a strong decrease in cell viability as a response to nanoparticle exposure. Incubation times of ≤4 h are sufficient to induce dramatic losses in cell viability after an additional induction period of 4−12 h. Mapping the temporospatial distribution of dead cells in the Caco-2 cell monolayer using optical microscopy reveals that the nanoparticles induce apoptosis in individual cells, which then propagate across the cell monolayer through a "bystander killing effect". Addition of catalase, which selectively decomposes hydrogen peroxide, leads to a significant decrease in apoptosis levels, indicating that hydrogen peroxide causes the spread of apoptosis across the monolayer. Our findings confirm that ingested nonbiodegradable nanoparticles represent a potential health risk due to their detrimental impact on the intestinal membrane by destroying their barrier protection capability over time.

KEYWORDS: nanotoxicity · apoptosis · bystander killing · engineered nanomaterials · oxidative stress · nano−bio interface

Due to their small size and large surface-to-volume ratio, engineered nanomaterials have unique properties that are different from those of the corresponding bulk material and enable new applications in catalysis,[1] electronics,[2] photonics,[3] and medicine.[4] The large surface-to-volume ratio of the nanomaterials, however, also creates more potential for toxic interactions.[5−7] Consequently, even for materials with overall low chemical reactivity and thus low chemical toxicity, potential dangers are related to morphological parameters such as the size and shape as well as to surface properties and charge. Although our understanding of the interactions of engineered nanomaterials with cells and tissue is incomplete, engineered nanomaterials are already used in consumer products including electronics, cosmetics, and automotive and medical products, and the number of applications in a wide field of industries is steadily increasing. If the number of nanoparticle applications develops as projected,[5] a large-scale distribution of engineered nanomaterials in the environment is realistic, resulting in significant exposure levels for humans. To assess the potential threat of the engineered nanomaterials, to develop effective treatment strategies after exposure, or to "engineer-out" potential hazardous properties in engineered nanomaterials, a fundamental understanding of the interactions between nanoparticles and living cells is mandatory.

The exact nature of the interactions between nanoparticles and cells depends on the nanoparticle exposure route, as this will determine the point of contact between human tissue and nanomaterials. Potential routes of nanomaterial exposure include inhalation, dermal contact, and ingestion.[8−10] During digestion of food, the transit time through the small intestine is about 4−8 h.[11] Hence on ingestion, nanomaterials reach the gastrointestinal tract and remain in contact with the intestinal epithelium for about 4−8 h. In the gastrointestinal tract, epithelial cells form a monolayer lining the intestinal lumen, and this epithelium forms a barrier that separates the sterile body interior from the harsh conditions of the lumen. Abnormal intestinal barrier function,

*Address correspondence to bmr@bu.edu.

Received for review August 27, 2009 and accepted June 08, 2010.

Published online June 18, 2010.
10.1021/nn100389a

specifically increased intestinal permeability, has been indicated in a series of intestinal diseases, most notably inflammatory bowel diseases including Crohn's disease.[12] The potential impairment of the intestinal membrane through nonbiodegradable nanomaterials could represent a pathogenic link between nanoparticle exposure and inflammatory bowel disease and raises further concerns about human exposure to engineered nanomaterials.

Simple intestinal epithelium consists of a layer of polarized cells in which each cell has two distinct surfaces: the apical surface facing the lumen and the basal surface facing the serosal environment. The individual neighboring cells have tight junctions which connect the individual enterocytes into a functional membrane. The intestinal membrane can be emulated by Caco-2 cells grown on a porous support. The cells form a monolayer of polarized epithelial cells with tight junctions that have an enterocyte-like morphology and express brush-border enzymes.[13] The Caco-2 system is an established enterocyte *in vitro* model system which has been widely used in the past to develop effective carriers for enhanced oral uptake of drugs and vaccines.[14,15] It has been shown that Caco-2 cells absorb[16] and transcytose[17,18] nanoparticles in the 20 −100 nm size range. By co-culturing Caco-2 cells with microfold cells, better known as M cells, the Peyer's patch tissue can be simulated.[19,20] The sparsely distributed M cells sample and transcytose antigens from the lumen of the small intestine and present them to lymphocytes on the basal side. It has been shown that the Peyer's patch regions also play a significant role in the gastrointestinal uptake of nano- and micrometer-scaled particles.[16,21−29] Another gastrointestinal uptake mechanism that has been observed is persorption,[30] which refers to the paracellular absorption of nano- and microparticles through the gut lumen into the body. In paracellular absorption, the nanoparticles are not transported across the cells as in transcytosis but instead pass between the cells. Persorption was found to occur efficiently through breaks in the tips of villis or through degrading and extruding enterocytes.[25] This observation, however, raises the question whether nanoparticle exposure can enhance persorption by damaging enterocytes and underlines the need for a better understanding of the mechanism by which nanomaterials potentially impact the stability and integrity of the intestinal membrane as a whole.

The ability of individual cells in the intestinal membrane to interact and communicate can be expected to have important implications for the toxicity of nanomaterials. This is cumbersome since there is experimental evidence that even nanoparticles with low chemical reactivity and toxicity can induce cell death. TiO_2 nanoparticle exposure, for instance, is associated with an increase in reactive oxygen species (ROS) in human airway epithelial cells (BEAS-2B), which triggers the activation of cytosolic caspase-3 and chromatin condensation.[31] In bronchoalveolar carcinoma-derived cells (A549), ZnO nanoparticles induce elevated levels of ROS, resulting in lipid peroxidation, cell membrane leakage, and oxidative DNA damage.[32] *A priori* it cannot be excluded that in a network of interacting cells (as in the case of an epithelial membrane) nanoparticle-induced cell death signaling spreads between adjacent cells. One potential outcome could be a rapid propagation of apoptosis across the membrane even at comparatively low nanoparticle concentrations which could compromise the intestinal membrane integrity.

As a first step toward an improved understanding of the nanoparticle−enterocyte interactions in the intestinal membrane, we will record a baseline for the effect of nonbiodegradable nanoparticles on the cell viability and integrity of a monolayer of differentiated Caco-2 cells. We deliberately chose nanoparticles made from a material with low chemical reactivity for these studies: polystyrene (PS). The overall low chemical toxicity[24] of the applied particles enabled us to investigate the nanotoxicity arising from the size and surface chemistry and nonbiodegradable nature of the particles. Our studies are motivated by the need for a better understanding of the mechanisms of nanoparticle−cell interactions in the intestinal epithelium as well as by the existing challenge of developing functional nanoparticles with low cytotoxicity for biomedical applications.[33] PS nanoparticles are candidates for nonviral gene delivery in gene therapy[34] as they can be synthesized with narrow size distributions over a large size range with defined surface functionalities. A quantitative understanding of the impact of specific nanoparticle material properties on the intestinal epithelium will advance our understanding of the threats related to an oral administration of these nanomaterials.

RESULTS AND DISCUSSION

Quantification of Nanoparticle Uptake. In all of our studies, we used fluorescent PS nanoparticles because they enable a convenient localization after cellular uptake using confocal laser scanning microscopy. In the first set of experiments, we characterized the uptake efficiency of three different nanoparticles: carboxylic-acid-functionalized 20 nm (20_{carb}) and 40 nm (40_{carb}) PS particles and amino-functionalized 40 nm particles (40_{amin}). This choice of particles enabled us to test the effect of particle size and surface chemistry on the uptake efficiency of small spherical PS particles. In the cell culture medium (pH 7.4) used for the uptake experiments (see Materials and Methods), 40_{amin} particles are partially protonated whereas the 20_{carb} and 40_{carb} particles are partially deprotonated. Zeta potential measurements show that, under these conditions, the carboxylic-acid-functionalized nanoparticles are negatively charged ($\zeta = -30 \pm 5$ mV) and the amine beads are positively charged ($\zeta = 28 \pm 10$ mV).

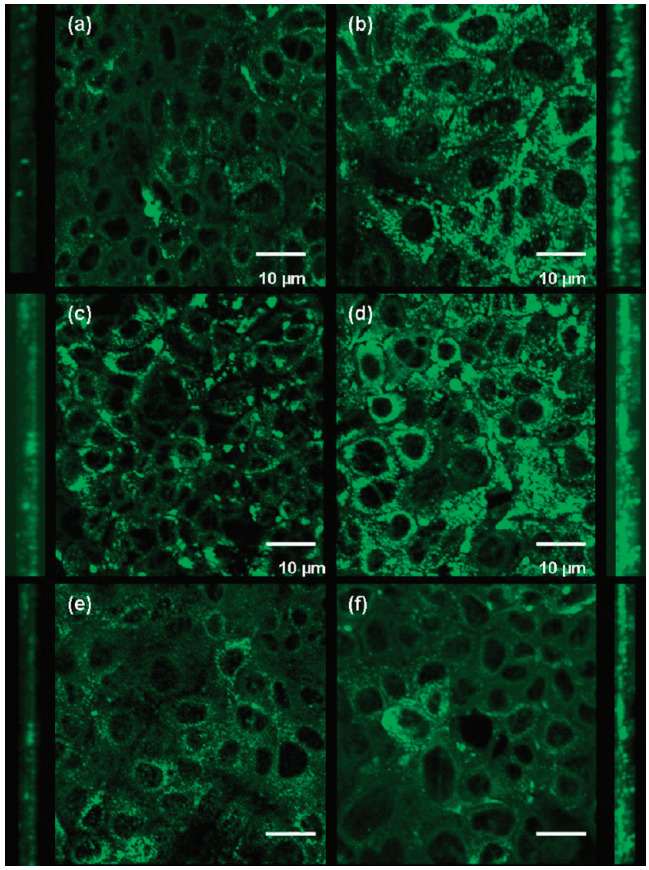

Figure 1. Confocal microscopy shows efficient uptake of fluorescent PS nanoparticles into the cytoplasm of Caco-2 cells. Whereas the nucleus remains dark, the cytoplasm shows a high degree of fluorescence. The figure shows a comparison between different concentrations of nanoparticles added to the monolayer: (a) 0.3 nM, 20_{carb} PS nanoparticles, (b) 6.6 nM, 20_{carb} PS nanoparticles, (c) 0.3 nM, 40_{carb} PS nanoparticles, (d) 6.6 nM, 40_{carb} PS nanoparticles, (e) 0.3 nM, 40_{amin} PS nanoparticles, (f) 6.6 nM, 40_{amin} PS nanoparticles. The images also show, in the side panels, side views of scans through the respective monolayers. The cells exhibit intense areas of fluorescence throughout the cytoplasm for both 0.3 and 6.6 nM particle solutions.

Membranes of differentiated Caco-2 cells that were considered intact based on trans-epithelial electrical resistance (TEER)[35] measurements were incubated with the nanoparticles for 16 h under growth conditions in the incubator at 37 °C and then fixed and imaged using confocal laser scanning microscopy. As we discuss in more detail below, the viability of the Caco-2 cells started to decrease when the particle concentration was raised to above 0.3 nM (corresponding to 0.8 μg/mL for 20 nm particles and 6.4 μg/mL for 40 nm particles), and at a concentration of 6.6 nM (17.5 and 139.9 μg/mL), the cell viability dropped to below 50% in the case of the carboxylic-acid-functionalized particles. We focused in our investigation of the cell−nanoparticle interactions primarily on this concentration range where distinct changes in the cell viability become apparent.

The confocal sections in Figure 1a−f show clear fluorescence staining of the cells, indicative of nanoparticle uptake, for both 0.3 and 6.6 nM solutions of all investigated PS nanoparticles. A quantitative comparison of the relative cytoplasmic nanoparticle concentrations is difficult based on the fluorescence images in Figure 1 because the investigated particles differ in size and dyes. Instead, we calculated relative uptake efficiencies by integrating the fluorescence intensities over all confocal sections through a Caco-2 monolayer and then normalizing (i) by the number of cells in the scan and (ii) by the fluorescence intensity of a 10 nM solution of the corresponding PS nanoparticles recorded in a fluorimeter under defined conditions. The highest calculated efficiency was set to 1, and the efficiencies for the other particles were scaled accordingly. The resulting relative uptake efficiencies are plotted in Figure 2.

The 20_{carb} particles have overall the highest uptake efficiency at 6.6 nM and are uptaken by a factor of ~5 more efficiently than the 40_{carb} particles, whose uptake efficiency is approximately a factor of 2 better than that of the 40_{amin} particles. The uptake efficiencies for 0.3 nM nanoparticle solutions are lower by a factor of ~2, but the overall trends between the particles remain the same as those observed for 6.6 nM solutions.

Cellular Distribution of Uptaken PS Nanoparticles. We probed the distribution of the uptaken PS nanoparticles within individual cells using confocal microscopy. Optical sectioning using *z*-scans through individual ~10 μm thick cells are shown as side bars to Figure 1a−f. These scans show large fluorescent agglomerates that are spread throughout the cytoplasm, indicating collection of endocytosed nanoparticles into endosomes or lysosomes.[36,37] Interestingly, even after an incubation time of 16 h, we did not observe a systematic enrichment of the fluorescent particles on the basal side, which argues against an efficient transcytosis of the particles on the time scale of our experiments. We also probed the solution

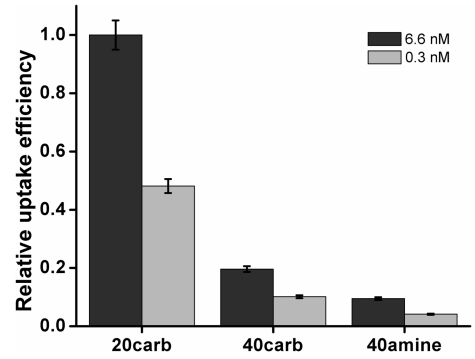

Figure 2. Relative uptake efficiencies as determined through confocal microscopy (see text) for two PS nanoparticle concentrations in the growth medium (0.3 and 6.6 nM).

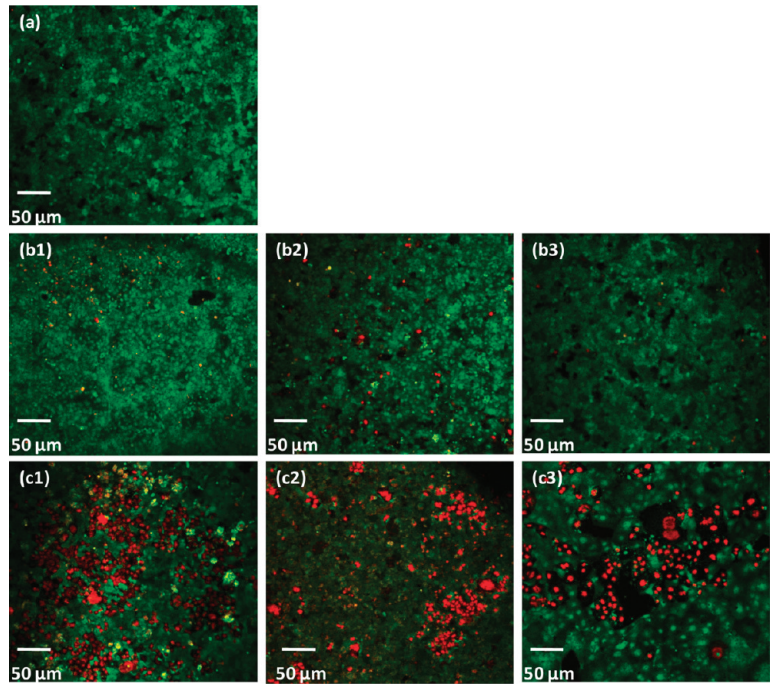

Figure 3. Live/dead assay for Caco-2 cell monolayer after 16 h of incubation with PS nanoparticles at different concentrations. (a) Control without PS nanoparticles (b1) 0.3 nM of 20_{carb}, (b2) 0.3 nM of 40_{carb}, (b3) 0.3 nM of 40_{amin}, (c1) 6.6 nM of 20_{carb}, (c2) 6.6 nM of 40_{carb}, (c3) 6.6 nM of 40_{amin}.

in the basal compartment for fluorescence but did not detect any, confirming that transcytosis rates were low.

Effect of Nanoparticle Concentration, Surface Chemistry, and Particle Size on Cell Viability. Having shown that the PS nanoparticles are uptaken by the cells and that the effective cytoplasmic nanoparticle concentration depends on the nanoparticle surface chemistry, we set out to investigate how nanoparticle exposure impairs the viability of Caco-2 cells. Previous studies have indicated that PS particles with 400 nm diameter significantly affect the cell viability of Caco-2 cells, and one of these studies reported excessive cytokine release as a response to PS nanoparticle exposure.[38,39] In our current work, we extend the scope of these studies by investigating the impact of significantly smaller PS particles with diameters between 20 and 40 nm and with different surface chemistries on the cell viability of Caco-2 cells. Fluorescence microscopy in combination with appropriate live/dead cell stains enabled us to monitor the temporospatial distribution of dead cells in a monolayer of Caco-2 cells that is incubated with growth medium containing nanoparticles at a defined concentration. Optical microscopy with single cell resolution is particularly useful for mapping specific patterns of dead cells in the cell monolayer and for monitoring how these patterns evolve as a function of space and time. In the epithelial membrane, the individual cells are not independent from each other but coupled through intercellular interactions, and the temporospatial distribution of dead cells provides some information about how these interactions are influenced by the nanoparticles.

In a first set of experiments we investigated the influence of the particle concentration and surface charge on the cell viability. To that end, Caco-2 cells were incubated with PS nanoparticle solutions of various concentrations (0.3−6.6 nM) in growth medium for 16 h. Then the cells were fixed and analyzed after live/dead staining in the fluorescence microscope (for details, refer to the Materials and Methods section). We show representative fluorescence images for a control sample (incubation for 16 h without nanoparticle exposure) in Figure 3a. Images for two 20_{carb} nanoparticle concentrations (0.3 and 6.6 nM) after 16 h incubation are shown in Figure 3b1,c1. The images for 0.3 and 6.6 nM solutions of 40_{carb} particles are shown in Figure 3b2,c2, and the images of 40_{amin} particles are shown in Figure 3b3,c3. Live cells appear green, and dead cells appear red. We note that the colors in Figure 3 arise exclusively from the live/dead stain. The fluorescence of the PS nanoparticles could be suppressed using appropriate filter combinations. From optical inspection of Figure 3, it becomes immediately clear that the cell viability decreases with increasing nanoparticle concentration. In addition, the cytotoxic effect of the nanoparticles is also prominent through some cell detachment from the membrane. We observe a number of large blank spots in the membrane in Figure 3c1−c3, which are absent in the control samples without nanoparticle exposure. This finding is a first indication of nanoparticle-induced apoptosis in the cell monolayer since apoptotic cells have been observed before to detach from growth substrates as well as from neighboring cells.[40] Figure 3b,c shows overall similar trends for all investigated PS

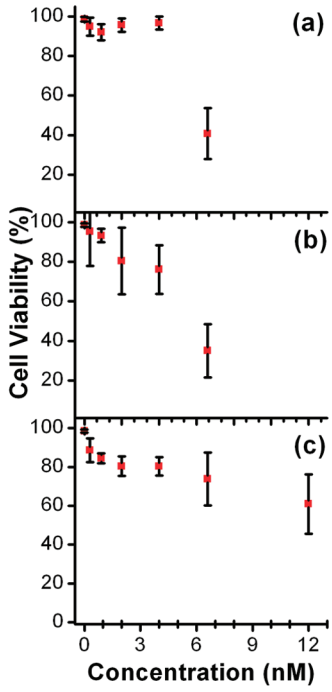

Figure 4. Cell viability as a function of concentration for (a) 20_{carb}, (b) 40_{carb}, and (c) 40_{amin} PS nanoparticles. The incubation time was constant (16 h). Results are expressed as percentage of cells referred to the control. Values are means ± standard deviation (SD) of 10 experiments.

nanoparticles. A detailed comparison of the influence of nanoparticle size and charge as a function of particle concentration requires a quantitative analysis of the cell viability. To that end, we computed the ratio of dead cells on the membranes after a 16 h incubation period. The results of 10 independent experiments are plotted as a function of particle concentration in Figure 4. For the 20_{carb} particles, we observed a broad concentration range across which the particles do not significantly affect cell viability. For concentrations ≤4.0 nM, the cell viability remains >90%. At 6.6 nM, the cell viability then suddenly drops to ~40%. For the 40_{carb} particles, the cell viability shows a gradual decrease already at lower particle concentrations. At a concentration of 4.0 nM, the cell viability has decreased to ~78%. A further increase of the particle concentration in the growth medium results in a further large drop in cell viability down to ~35%. In the case of the 40_{amin} nanoparticles, we do not observe a decrease in cell viability of comparable magnitude as observed for the carboxylic-acid-functionalized particles in the investigated concentration range of ≤12.0 nM. The cell viability exhibits a continuous gradual decrease down to ~62% at a particle concentration of 12.0 nM. This value is approximately a factor of 2 higher than that observed for 6.6 nM solutions of the 40_{carb} particles, underlining a clear dependence of the particle cytotoxicity on the surface chemistry of the particles.

Overall, the observed trends indicate that the 40_{amin} particles have a smaller impact on the cell viability of the investigated Caco-2 cells than the 40_{carb} and 20_{carb} PS particles. Our studies show a strong influence of the particle size on the cell viability. Although the uptake efficiency is highest for the 20_{carb} particles, the effect of these particles on the cell viability is low until a threshold concentration of 6.6 nM in the medium is reached. In contrast, the larger 40_{carb} particles exhibit a measurable response already at lower particle concentrations, despite the lower uptake efficiency for the larger particles.

Time Dependence of Nanoparticle-Induced Changes in the Cell Viability. The performed investigations of the cell viability as a function of particle concentration at a constant incubation time (16 h) revealed that PS nanoparticles can have significant detrimental effects on a monolayer of enterocyte-like Caco-2 cells. For a realistic assessment of the nanoparticle-related threat, the interaction dynamics needs to be considered, as well. Ingested food stays in contact with the small intestine for about 4−8 h, and we assume that the nanoparticles remain in the small intestine for the same period of time in a first approximation.[11] We quantified the impact of nanoparticle exposure as a function of time by calculating the cell viability of Caco-2 cells at fixed incubation times during a total observation time of 16 h. In Figure 5, the resulting cell viabilities for 6.6 nM solutions of nanoparticles are plotted as a function of time. We included parabolic fits as red lines to the experimental data for the 20_{carb} (Figure 5a), 40_{carb} (Figure 5b), and 40_{amin} (Figure 5c) particles. In all three cases, the cell viability decreases over the total observation time. Consistent with our studies of the concentration-dependent effect of nanoparticle exposure, we find that over the total observation time of 16 h the carboxylic-acid-functionalized nanoparticles decrease the cell viability more strongly than the amino-functionalized particles.

The dynamics of the loss in cell viability shows interesting differences between the investigated particle types. For the 40_{carb} particles, the initial decrease in cell viability is overall low in the first 3−4 h, but after this induction period, the cell viability decreases rapidly. In contrast, for the 20_{carb} particles, the differences in the slope of the cell viability *versus* time plot between short and long incubation times are less pronounced, and we observe a steady drop in the cell viability already for incubation times <4 h. The decrease in cell viability for the 20_{carb} particles is almost linear over the observed incubation time. The differences between the 20_{carb} and 40_{carb} particles at short incubation times indicate that the smaller carboxylic-acid-functionalized particles are more potent at shorter incubation times than the larger particles. The steeper slope for short incubation times could arise from an intrinsically higher cytotoxicity of smaller particles or could be a direct consequence of the higher uptake rates for the smaller particles. As shown in Figure 2, the 20_{carb} particles have the highest

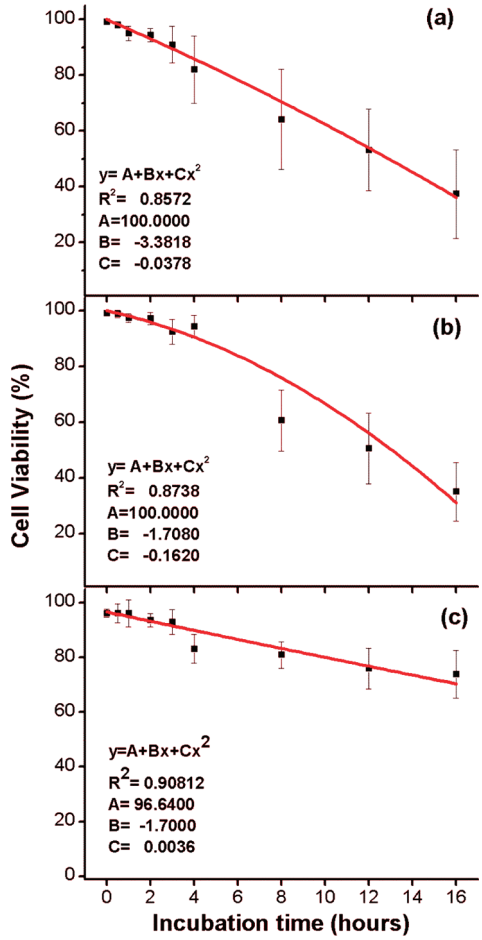

Figure 5. Cell viability as a function of time for Caco-2 cells incubating in growth medium containing 6.6 nM (a) 20_{carb}, (b) 40_{carb}, and (c) 40_{amin} PS nanoparticles. Results are expressed as percentage of cells referred to the control. Values are means ± SD of 10 experiments.

uptake efficiency of all investigated particles, and we expect the cellular nanoparticle concentration to grow fastest for 20_{carb} PS particles. Overall, the decrease in cell viability occurs slowest for the 40_{amin} particles for which we observed the lowest uptake efficiency, suggesting that the observed cell viability dynamics is correlated with the nanoparticle uptake dynamics.

For all investigated particles, independent of the observed differences as a function of particle size and surface chemistry, we observe a substantial drop in cell viability on the time scales relevant for nanoparticle−epithelial cell interactions of 4−8 h. After 4 h, the fitted cell viability has decreased to 82% for the 20_{carb} particles, to 90% for the 40_{carb} particles, and to 87% in case of the 40_{amin} particles. After 8 h, the fitted viabilities have dropped to 63% for the 20_{carb} particles, 65% for the 40_{carb} particles, and 82% for 40_{amin} particles.

All data in Figure 5 were obtained through continuous incubation of the cells in the nanoparticle-containing medium. We wondered if this continuous incubation in the presence of nanoparticles is necessary for the observed large decline in cell viability or if a

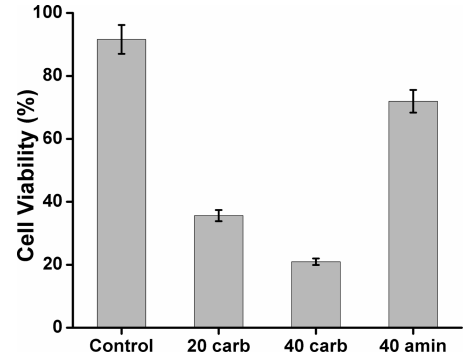

Figure 6. Histogram of cell viability observed for 6.6 nM solutions of different PS nanoparticles. In this experiment, the PS nanoparticle-containing medium was exchanged with PS nanoparticle-free medium after 4 h. The cells exchanged with PS nanoparticle-free medium were then incubated for another 12 h. The reported values are mean ± SD of 10 experiments.

shorter exposure to the nanoparticles followed by an incubation in the absence of nanoparticles leads to similar drops in cell viability. To test this hypothesis experimentally, we incubated Caco-2 with solutions of 6.6 nM nanoparticles for 4 h and then replaced the nanoparticle-containing medium with common growth medium and continued incubation in this PS nanoparticle-free medium until a total incubation time of 16 h was reached. Then the cells were fixed and analyzed using a fluorescent live/dead cell assay. The resulting cell viabilities, which are histogrammed in Figure 6, are very similar to those obtained under continuous incubation conditions. This observation proves that the nanoparticle uptake that occurs on the biologically relevant time scale of 4 h is sufficient to induce cellular processes that ultimately terminate in cell death even without further exposure to nanoparticles. This model can also explain the strong parabolic time dependency especially for the 40_{carb} particles for which an initial induction period with slower decay of the cell viability is followed by a faster decline.

The picture that emerges from our experiments so far is that carboxylic-acid-functionalized particles impair the cell viability of Caco-2 cells faster and more strongly than amino-functionalized particles. Exposure times on the length scale of the transit time of nanoparticles in the small intestine (≤4 h) are sufficient to cause dramatic losses in the cell viability after an induction period of 4−12 h.

Apoptosis *versus* Necrosis. The observed significant decrease in cell viability as a function of PS particle size, surface chemistry, and concentration prompted our interest in the mechanisms underlying the observed cell death in the Caco-2 monolayers. In principle, the observed nanoparticle-induced processes can be apoptotic or necrotic. Apoptosis refers to an active pattern of cell death which is activated by intra- or extracellular signals, whereas necrosis refers to a passive form of dying induced by some physical, chemical, or biological

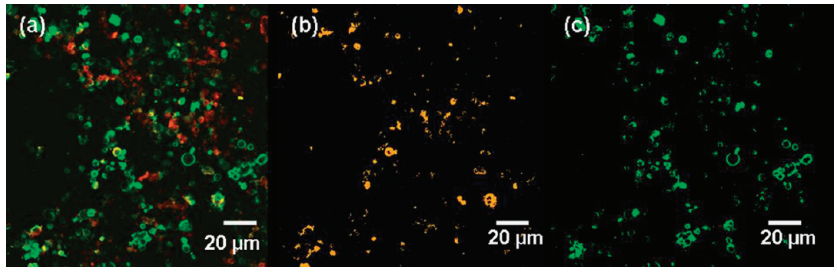

Figure 7. (a) Co-staining of a Caco-2 cell monolayer with fluorescently labeled annexin V (green) and propidium iodide (red). (b) Digital image highlighting all areas where red and green superimpose. (c) Digital image in which all areas stained by propidium iodide are blanked out, leaving only areas that are exclusively stained by annexin V.

factors.[41] To determine if the observed cell death was apoptotic or necrotic, we first performed annexin V and propidium iodide co-staining experiments. Propidium iodide is a DNA stain, whereas annexin V binds with high affinity to phosphatidylserine, which is translocated to the cell surface soon after induction of apoptosis.[42] Cells that stain with annexin V but not with propidium iodide have intact plasma membranes and show phosphatidylserine externalization. This behavior is a strong indicator of early stage apoptosis.

Figure 7a shows a monolayer of Caco-2 cells that have been incubated with 20_{carb} nanoparticles at a concentration of 6.6 nM for 16 h and then co-stained with propidium iodide (red) and annexin V (green). Figure 7a contains both red and green areas, and it is necessary to analyze the distribution of these areas in more detail. Figure 7b is a digitally rendered image that shows only those areas in which red and green co-localize. The cells in these areas are in a state of either late apoptosis or necrosis; a further differentiation is not possible based on Figure 7b alone. Additional information is, however, provided by Figure 7c, which only contains those areas that are stained by annexin V but not by propidium iodide, and thus identifies cells that are in a state of early apoptosis. Together the findings in Figure 7b,c suggest the coexistence of different stages of apoptosis (early and late) in the Caco-2 cell monolayer after an incubation with PS nanoparticles for 16 h.

Another frequently used indicator of apoptosis is a decrease in the mitochondrial membrane potential.[43] Our approach to probe the mitochondrial transmembrane potential in Caco-2 cells after nanoparticle exposure was based on a conventional fluorescent Mitotracker dye, which shows a bright red fluorescence in the presence of a mitochondrial transmembrane potential. In apoptotic cells, the mitochondrial membrane becomes permeable and the red fluorescence decreases. The staining pattern in Figure 8 confirms reduced mitochondrial transmembrane potential in Caco-2 cells that translocate phosphatidylserine. This behavior is indicative of apoptosis.

Caspases play a central role in apoptosis, and increased caspase activity indicates apoptosis.[44] In an additional apoptosis assay, we therefore compared the caspase-3 activity in Caco-2 cells that were incubated with PS nanoparticles and unexposed control cells. The caspase-3 activity was enhanced by a factor >5 in Caco-2 cells that were incubated with PS nanoparticles (Figure S1 in Supporting Information). Together with the observed phosphatidylserine externalization and the reduced mitochondrial transmembrane potential, the increased caspase activity is evidence for PS nanoparticle-induced apoptosis in monolayers of Caco-2 cells. Although we cannot exclude that individual cells undergo necrosis, the results of the performed apoptosis are consistent with apoptosis as the major cell death mechanism for the Caco-2 cells.

Apoptosis is a natural and well-controlled process which ensures that cells are replaced when they malfunction or become diseased, and it therefore plays an important role in maintaining a correct balance between cell proliferation and death. Excessive apoptosis as response to PS nanoparticle exposure as observed in our experiments here is a clear sign of nanoparticle-induced cell stress that triggers cellular responses resulting in cell death. PS particles have an overall low chemical toxicity, however, *a priori* it cannot be excluded that the dye leaches out of the fluorescent PS nanoparticles used in our studies and causes the observed apoptosis. We therefore performed control experiments in which we confirmed that the supernatant from the fluorescent PS nanoparticles that were cleaned by centrifugation showed no significant change in cell

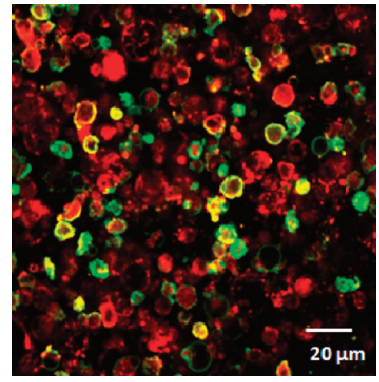

Figure 8. Mitochondrial transmembrane potential assay using fluorescently labeled annexin V and Mitotracker dye. Apoptotic cells with reduced transmembrane potential are bright green with annexin V stain and dull red with mitochondrial stain, as opposed to healthy cells being dull green and bright red.

viability (see Supporting Information, Figure S2). On the basis of these control experiments, we exclude a chemical toxicity of the PS particles as cause for the observed cell death. Instead, we attribute the observed high levels of apoptosis for Caco-2 cells after PS nanoparticle exposure to cellular stress induced by the uptake of nonbiodegradable nanoparticles. In order to obtain additional information about the nature and the underlying mechanisms of the observed cellular stress in the Caco-2 monolayer, we investigated the temporospatial evolution of apoptosis in the Caco-2 intestinal model next.

Temporospatial Evolution of Apoptosis in a Caco-2 Monolayer. Unlike for individual cells, in a system of interacting cells such as the epithelial membrane, the individual cells are influenced by communication and direct interactions with their neighboring cells. These interactions can occur through gap junctions and tight junctions as well as through the release of signaling molecules into the cellular environment.[45] Consequently, the response of a monolayer of cells in which the fate of each individual cell is intertwined with that of its neighbors can differ from that of individual cells. Optical inspection of the Caco-2 monolayer after fluorescent staining in Figure 3 suggests that the apoptotic cells are not homogenously distributed over the monolayer, but that the probability of finding an apoptotic cell varies significantly as a function of the location of the membrane. The probability of finding an apoptotic cell is higher near another apoptotic cell than anywhere else in the monolayer. To confirm this hypothesis of apoptotic clustering in Caco-2 cultures, we performed statistical analysis using the Hopkins statistical method.[46] This statistics tests spatial randomness by comparing nearest neighbor distances from random points and randomly chosen probes (here, apoptotic cells) and provides an *H* factor as quantitative measure for clustering (see Materials and Methods section).[46] The resulting *H* values lie in the interval [0, 1]. For randomly distributed apoptotic cells, the expected value is 0.5, whereas for clustered apoptotic cells, the value is closer to 0 or 1.

The Hopkins statistics for the distribution of apoptotic cells in monolayers of Caco-2 cells after incubation in medium of 6.6 nM nanoparticles are plotted in Figure 9. For all three investigated PS particles, the Hopkins statistics is clearly shifted with regard to a random distribution, confirming that the apoptotic cells are clustered. In developing and renewing systems, clustering of apoptotic cells is often caused through bystander killing,[47,48] in which a primary apoptotic cell induces apoptosis in viable neighboring cells. Bystander killing implies that a few primary apoptotic cells can induce and propagate apoptosis across the entire intestinal membrane. Several chemical signals can be sent either by extracellular matrix or through the tight junctions from primary apoptotic cells to trigger apoptosis in the neighboring cells.[48] However, in the case of an epithelial cell monolayer like

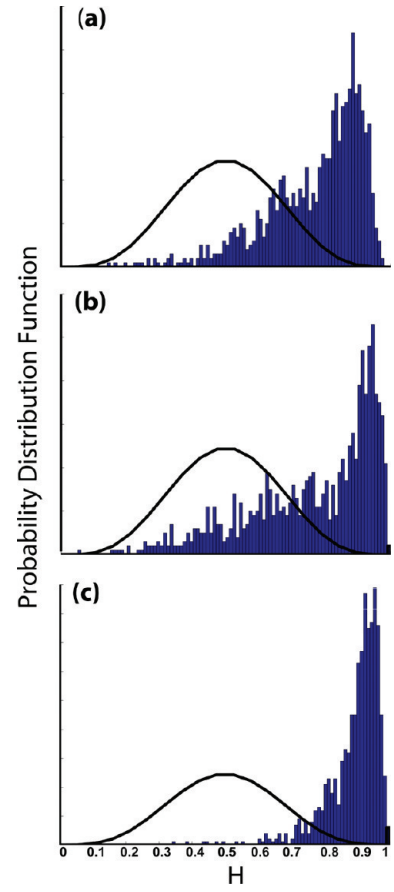

Figure 9. Hopkins test for the clustering of apoptotic cells in Caco-2 cell monolayers for (a) 20_{carb}, (b) 40_{carb}, and (c) 40_{amin}. The cells were incubated with medium containing 6.6 nM PS nanoparticles and analyzed after a total incubation time of 16 h. The strong shift of the distribution to the right compared with the Gaussian distribution (black) indicates strong cell clustering.

Caco-2, the tight junction proteins break down when the cells undergo an apoptotic death.[49] Consequently, we will first focus on an extracellular mechanism as a potential trigger for the observed apoptosis.

Apoptosis has been associated with oxidative stress in biological systems, and previous studies have indicated a link between nanoparticle exposure and elevated levels of oxidative stress.[50−55] Oxidative stress results from an imbalance between oxidants and antioxidants in cells exposed to nanoparticles. One strong oxidant in the cellular environment is hydrogen peroxide (H_2O_2), which is produced in the mitochondria, cytosol, and peroxisomes as a product of oxidases and superoxide dismutase.[56] Among biologically relevant reactive oxygen species, hydrogen peroxide is a promising candidate for a cell death signal messenger since it is comparatively stabile with a half-life on the order of seconds. H_2O_2 readily penetrates cell membranes, and this ability together with its relatively long lifetime allows the molecule to diffuse into a nearby cell and to react with its cellular components.[48] To verify that H_2O_2 is involved in the observed spread of apoptosis across the membrane, we added catalase to the nanoparticle-containing medium.[48,57] This enzyme cata-

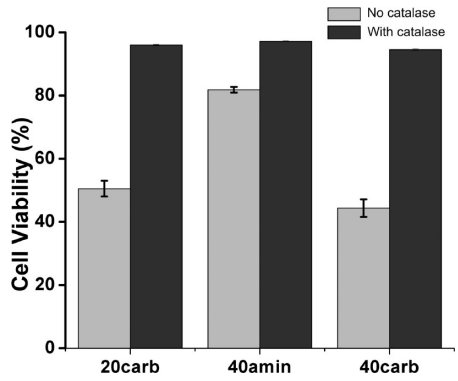

Figure 10. Cell viability for Caco-2 cells incubated with PS nanoparticles in the presence and absence of catalase. The cells were incubated with 6.6 nM solutions of the different nanoparticles for 16 h. Values are means ± SD of 10 experiments.

lyzes the decomposition of H_2O_2 into $^1/_2O_2$ and H_2O. Since the catalase cannot cross the plasma membrane and diffuse into cells,[58] it only removes H_2O_2 that has been released by the cells into the extracellular environment. The comparison of the cell viabilities measured with and without catalase in Figure 10 shows that catalase addition leads to a strong reduction in nanoparticle-induced apoptosis and confirms that H_2O_2 is the signal mediating the propagation of apoptosis upon nanoparticle exposure.

On the basis of these observations, we propose the following model of nanoparticle-induced apoptosis in the Caco-2 monolayer. Nanoparticle uptake induces oxidative stress in the Caco-2 monolayer from primary apoptotic Caco-2 cells, which results in H_2O_2 release. The released oxidant further increases the oxidative stress in the immediate vicinity and triggers apoptosis in neighboring, secondary cells that are in reach through diffusion on the time scale of its lifetime. The observed clustering indicates that, in the majority of the apoptotic cells, cell death is not immediately caused by the uptaken PS nanoparticles but instead results from increased levels of H_2O_2 released by primary apoptotic cells in the monolayer. Overall, the observation of nanoparticle-induced oxidative stress in a monolayer of Caco-2 enterocyte-like cells and the observed H_2O_2-mediated propagation of apoptosis across the monolayer confirm concerns about the potential health threat of ingested nanomaterials.

CONCLUSIONS

In this work, we investigated the impact of 20 and 40 nm carboxylic acid and 40 nm amino-functionalized PS particles on a monolayer of enterocyte-like Caco-2 cells. We found that the uptake efficiency is higher for the negatively charged carboxylic-acid-functionalized particles than for the positively charged amino-functionalized particles and higher for smaller 20 nm than for larger 40 nm PS nanoparticles. All investigated particles lead to a decrease in cell viability of Caco-2 cells, but the carboxylic-acid-functionalized particles decrease the cell viability faster and stronger. Following the trends for uptake efficiency, we find that the smaller particles impact the cell viability more strongly than larger particles. Our studies show that exposure time of the length scale of the residence time of nanoparticles in the small intestine are sufficient to cause dramatic losses in the cell viability. The initially uptaken nanoparticles induce cellular processes that terminate in cell death within 4−12 h. The dead cells are found to cluster in the cell monolayer as a result of nanoparticle-induced apoptosis in the vicinity of primary apoptotic cells, a process named bystander killing.[47] Oxidative stress in primary apoptotic cells results in the release of hydrogen peroxide into the extracellular environment, which then induces apoptosis in neighboring cells. The spread of apoptosis in the Caco-2 monolayer is efficiently suppressed in the presence of catalase, which catalyzes the decomposition of hydrogen peroxide to water and oxygen. Our studies show that nonbiodegradable nanoparticles have a significant impact on the cell viability in the Caco-2 intestinal membrane model by triggering apoptosis in individual cells, which then efficiently propagates across the entire membrane through release of a reactive oxygen species (hydrogen peroxide). The *in vitro* studies indicate that nanoparticle ingestion poses a health threat by inducing oxidative stress in the intestinal system. Like any *in vitro* system, the intestinal model system used in this work does not have the full functionality of the corresponding *in vivo* system. For instance, the intestinal epithelium is covered by a protective mucus layer which can influence the interactions between the nanoparticles and the intestinal membrane. This mucus layer is absent in our model system. The findings of our *in vitro* study are nevertheless important since they identify nanoparticle-induced oxidative stress in the intestinal epithelium as a potential health threat related to ingested nanoparticles. Further studies with improved *in vitro* and *in vivo* model systems will help to understand this risk in more detail.

MATERIALS AND METHODS

Cell Culture and General Experimental Procedures. The heterogeneous human epithelial colorectal adenocarcinoma cells, Caco-2 (American Type Culture Collection, ATCC, number: HTB-37), were grown in Dulbecco's modified minimum essential medium (DMEM) containing 25 mM glucose, 3.7 g of $NaHCO_3$ L^{-1} and supplemented with 4 mM L-glutamine, 10% fetal calf serum, 1% nonessential amino acids, penicillin (100 units mL^{-1}), and streptomycin (100 μg mL^{-1}) at 37 °C in an atmosphere of 5% CO_2 and 95% air at 90% relative humidity. After reaching 80% confluency, they were then seeded onto polyethylene filter cell culture chamber inserts. We used an accelerated Caco-2 differen-

tiation model provided by BD Biosciences. The 24-well insert systems were treated with type 1 rat tail collagen under conditions that allow *in situ* formation of large collagen fibrils. Caco-2 cells were seeded onto these inserts at 2×10^5 (cells/insert) in basal seeding medium (BD Biosciences) that was augmented with serum extender (MITO+, BD Biosciences) and were then incubated for 24 h. The medium on both sides of the membrane was subsequently exchanged with differentiation medium (Entero-STIM, BD Biosciences) and incubated for an additional 48 h. The membranes were ready for cytotoxicity assays on the third day.

The integrity of the cell membrane was tested by measuring the transepithelial electrical resistance (TEER) across the monolayer using a Millicell-ERS system ohm meter and a corresponding electrode system. The TEER values were measured prior to the experiment, and only membranes having TEER values $>200\ \Omega/cm^2$ were used for the experiment. A TEER value less than $150\ \Omega/cm^2$ indicates a compromised or a leaky membrane (according to the manufactures instructions, BD Biosciences). These membranes were discarded.

Twenty nanometer and 40 nm fluorescent polystyrene nanoparticles (FluoSpheres, Molecular Probes) were used that contained red fluorescent dyes (20_{carb} and 40_{amin}: λ_{exc}= 535 nm; λ_{em} = 575 nm) and (40_{carb}: λ_{exc}= 580 nm; λ_{em} = 605 nm) enclosed in the particles. We verified that the dyes did not leach out of the nanoparticles over the time period of our experiments. After incubation of the PS nanoparticles in neutral and acidic aqueous solutions for at least 12 h, the particles were spun down and the supernatant was tested for fluorescence. We did not detect any significant signal in neutral or acidic solutions. In a second control experiment, fluorescence nanoparticles were incubated for 16 h in growth medium. Then the particles were spun down, and the supernatant was tested for its cytotoxic effect by comparing the cell viability of Caco-2 cells incubated in the nanoparticle-treated buffer with controls incubated in pristine buffer. The nanoparticle-treated buffer did not lead to a decrease in cell viability (see Figure S2, Supporting Information).

The charge on these PS particles was determined through the particles' surface chemistry. Carboxylic-acid-functionalized particles are negatively charged, whereas amino-functionalized particles are positively charged in the growth medium (pH 7.4). The particles were sonicated for 1 min to separate the particles prior to use and then resuspended in the growth medium to yield colloidal solutions of final concentrations of 0.3, 0.9, 2.0, 4.0, and 6.6 nM. The solutions were added to the membranes and then incubated for 16 h. Finally, the cell viability was quantified using a live/dead cell assay (Invitrogen, USA). At least five membranes containing about 2×10^5 cells/insert were prepared and analyzed for each experiment. In order to observe the propagation of nanoparticle effect on the membrane in further detail, the cell viability was analyzed as a function of time, and samples were analyzed at 4, 8, 12, and 16 h for the highest nanoparticle concentration.

Visualization of Cellular Uptake of Nanoparticles. Three days after Caco-2 seeding (2×10^5 cells/insert), cells were transferred into growth medium containing nanoparticles and incubated at 37 °C in an atmosphere of 5% CO_2 for the specified amount of time ranging from 4 to 16 h. Cells were washed with phosphate buffered saline (PBS) and then fixed using a 4% aqueous solution of fresh paraformaldehyde, washed, and then visualized with an Olympus confocal laser scanning microscope (CLSM, Olympus Co. Ltd., Tokyo, Japan). All images were compiled using Image J software (NIH, USA) and are used as representatives of the original data.

Determination of Cell Viability. The effect of the PS nanoparticles on the cell viability as a function of particle charge, size, concentration, and incubation time was quantified using a commercial live/dead cell assay (Invitrogen, USA). The performed assay consists of calcein acetoxymethyl (calcein AM) and ethidium homodimer-1 (EthD-1). Live cells have intracellular esterases that convert nonfluorescent, cell-permeable calcein AM to the intensely fluorescent calcein (λ_{exc}= 495 nm; λ_{em}= 515 nm). Cleaved calcein is retained within cells. Dead cells have damaged membranes; EthD-1 therefore enters the damaged cells and becomes fluorescent after binding to nucleic acids. EthD-1 (λ_{exc} = 495 nm; λ_{em} = 635 nm) produces a bright red fluorescence in cells with damaged membrane or dead cells. The calcein AM and ethidium homodimer-1 mix is used to differentiate live (green) cells from dead (red) cells.

The live/dead assay was performed after exposing the Caco-2 cell monolayers to specified concentrations of PS nanoparticles (ranging from 0.3 to 6.6 nM) for specified incubation time (ranging from 4 to 16 h). The fluorescent dyes were mixed in PBS buffer and incubated with the cells for about 15 min. The cells were then fixed in 4% aqueous solution of fresh paraformaldehyde and washed. Confocal laser scanning microscopy was used to probe the uptake of the fluorescent nanoparticles as a function of time and concentration. Appropriate filter sets allowed independent visualization of PS nanoparticles (λ_{em} = 575/605 nm), live (λ_{em} = 515 nm), and dead cells (λ_{em} = 635 nm).

Apoptosis Assays. The dying cells were further differentiated into apoptotic and necrotic cells using different apoptosis assays. All assays were performed with Caco-2 cells that were incubated for 16 h with 20_{carb} PS nanoparticles at a concentration of 6.6 nM. Phosphatidylserine translocation was detected using the Vybrant Apoptosis Assay Kit #2 (Invitrogen, USA). The assay consists of Alexa488-labeled annexin V (λ_{exc}= 488 nm; λ_{em} = 525 nm), which is an anticoagulant having a high binding affinity to the phosphatidylserine in the cell membrane and the DNA stain propidium iodide. The kit was used according to the manufacture's protocol. Changes in the mitochondrial transmembrane potential were detected using a combination of Alexa488-labeled annexin V and the Mitotracker dye (Vybrant Apoptosis Assay Kit #11, Invitrogen, USA), whose red fluorescence intensity (λ_{exc}= 550 nm; λ_{em} = 595 nm) depends on the mitochondrial transmembrane potential. The kit was used according to the manufacture's instructions, and control experiments were performed that confirmed that fluorescence bleed-through from the 20_{carb} particles did not impair the ability to detect differences in the mitochondrial transmembrane potential. In a third assay, the caspase activity in Caco-2 cells was quantified using the EnzChek Caspase-3 Assay Kit #2 (Invitrogen, USA). This kit detects apoptosis by providing a reliable method for assaying caspase-3 activity. The basis for the assay is the rhodamine 110 derived substrate Z-DEVD-R110. This substrate is a nonfluorescent bisamide that is first converted by caspase-3 to the monoamide and then to the bright green fluorescent rhodamine 110 (λ_{exc}= 496 nm; λ_{em} = 520 nm). The kit was used according to the manufacturer's instructions.

Clustering Analysis Using the Hopkins Statistic. For spatial analysis of clustering, we use the complete spatial randomness (CSR)[59−61] hypothesis and calculate the Hopkins statistics.[46,62] It is a sensitive and dimensionless method that allows an easy comparison between different experiments.[61] This approach was used by Zhang *et al.* to analyze the clustering of immunolabels on a cell membrane.[61] Our analysis is based on the Matlab toolbox provided by Zhang *et al*. This program evaluates the nearest neighbor distances between random points and randomly chosen dead cells. The Hopkins statistic is defined as

$$H = \frac{U}{U + W}$$

with $U = \sum_{j=1}^{m} d^2(s_j,S)$ and $W = \sum_{k=1}^{m} d^2(p_k,S)$. Here m is the chosen number of random points $s_j = (x_j,y_j)$, and the chosen number of random dead cells of a set S with coordinates $p_k = (x_k,y_k)$. The parameter d is the interpoint distance. The H values lie in the interval between 0 and 1. In the case of spatial randomness event, $H = 1/2$. For clustering events, $H \approx 1$. After calculating the H values, the probability density function $f(H)$ is found as

$$f(H) = \frac{(1 - H)^{m-1}H^{m-1}}{(m - 1)!(2m - 1)!}$$

Finally, H (abscissa values) and $f(H)$ (ordinate values) are plotted together as histograms of the relative frequency distribution. For random dead cell distributions, the histogram of the relative frequency distribution assumes a Gaussian curve centered at $H = 0.5$. On the contrary, for clustered distribution, the

obtained histogram is shifted from the expected curve for random distribution.

Fluorescence Microscopy. Cell viability and apoptosis were quantified using a wide field fluorescent microscope (Olympus Co. Ltd., Tokyo, Japan) with appropriate filter sets to distinguish between the various dyes.

Supporting Information Available: Figures S1 and S2. This material is available free of charge *via* the Internet at http://pubs.acs.org.

REFERENCES AND NOTES

1. Daniel, M. C.; Astruc, D. Gold Nanoparticles: Assembly, Supramolecular Chemistry, Quantum-Size-Related Properties, And Applications toward Biology, Catalysis, And Nanotechnology. *Chem. Rev.* **2004**, *104*, 293–346.
2. Trindade, T.; O'Brien, P.; Pickett, N. L. Nanocrystalline Semiconductors: Synthesis, Properties, and Perspectives. *Chem. Mater.* **2001**, *13*, 3843–3858.
3. Barnes, W. L.; Dereux, A.; Ebbesen, T. W. Surface Plasmon Subwavelength Optics. *Nature* **2003**, *424*, 824–830.
4. Monsky, W. L.; Fukumura, D.; Gohongi, T.; Ancukiewcz, M.; Weich, H. A.; Torchilin, V. P.; Yuan, F.; Jain, R. K. Augmentation of Transvascular Transport of Macromolecules and Nanoparticles in Tumors Using Vascular Endothelial Growth Factor. *Cancer Res.* **1999**, *59*, 4129–4135.
5. Colvin, V. L. The Potential Environmental Impact of Engineered Nanomaterials. *Nat. Biotechnol.* **2003**, *21*, 1166–1170.
6. Oberdorster, G.; Oberdorster, E.; Oberdorster, J. Nanotoxicology: An Emerging Discipline Evolving from Studies of Ultrafine Particles. *Environ. Health Perspect.* **2005**, *113*, 823–839.
7. Tsuji, J. S.; Maynard, A. D.; Howard, P. C.; James, J. T.; Lam, C. W.; Warheit, D. B.; Santamaria, A. B. Research Strategies for Safety Evaluation of Nanomaterials, Part IV: Risk Assessment of Nanoparticles. *Toxicol. Sci.* **2006**, *89*, 42–50.
8. Borm, P. J. A.; Kreyling, W. Toxicological Hazards of Inhaled Nanoparticles—Potential Implications for Drug Delivery. *J. Nanosci. Nanotechnol.* **2004**, *4*, 521–531.
9. Kreyling, W. G.; Semmler-Behnke, M.; Moller, W. Health Implications of Nanoparticles. *J. Nanopart. Res.* **2006**, *8*, 543–562.
10. Papp, T.; Schiffmann, D.; Weiss, D.; Castranova, V.; Vallyathan, V.; Rahman, Q. Human Health Implications of Nanomaterial Exposure. *Nanotoxicology* **2008**, *2*, 9–27.
11. Degen, L. P.; Phillips, S. F. Variability of Gastrointestinal Transit in Healthy Women and Men. *Gut* **1996**, *39*, 299–305.
12. Weber, C. R.; Nalle, S. C.; Tretiakova, M.; Rubin, D. T.; Turner, J. R. Claudin-1 and Claudin-2 Expression Is Elevated in Inflammatory Bowel Disease and May Contribute to Early Neoplastic Transformation. *Lab. Invest.* **2008**, *88*, 1110–1120.
13. Hauri, H. P.; Sterchi, E. E.; Bienz, D.; Fransen, J. A. M.; Marxer, A. Expression and Intracellular-Transport of Microvillus Membrane Hydrolases in Human Intestinal Epithelial-Cells. *J. Cell Biol.* **1985**, *101*, 838–851.
14. Delie, F.; Rubas, W. A Human Colonic Cell Line Sharing Similarities with Enterocytes as a Model to Examine Oral Absorption: Advantages and Limitations of the Caco-2 Model. *Crit. Rev. Ther. Drug Carrier Syst.* **1997**, *14*, 221–286.
15. Pinto, M.; Robineleon, S.; Appay, M. D.; Kedinger, M.; Triadou, N.; Dussaulx, E.; Lacroix, B.; Simonassmann, P.; Haffen, K.; Fogh, J.; Zweibaum, A. Enterocyte-like Differentiation and Polarization of the Human-Colon Carcinoma Cell-Line Caco-2 in Culture. *Biol. Cell* **1983**, *47*, 323–330.
16. Desai, M. P.; Labhasetwar, V.; Walter, E.; Levy, R. J.; Amidon, G. L. The Mechanism of Uptake of Biodegradable Microparticles in Caco-2 Cells Is Size Dependent. *Pharm. Res.* **1997**, *14*, 1568–1573.
17. Koch, A. M.; Reynolds, F.; Merkle, H. R.; Weissleder, R.; Josephson, L. Transport of Surface-Modified Nanoparticles through Cell Monolayers. *Chembiochem* **2005**, *6*, 337–345.
18. Ragnarsson, E. G.; Schoultz, I.; Gullberg, E.; Carlsson, A. H.; Tafazoli, F.; Lerm, M.; Magnusson, K. E.; Soderholm, J. D.; Artursson, P. *Yersinia pseudotuberculosis* Induces Transcytosis of Nanoparticles across Human Intestinal Villus Epithelium *via* Invasin-Dependent Macropinocytosis. *Lab. Invest.* **2008**, *88*, 1215–1226.
19. Kerneis, S.; Caliot, E.; Stubbe, H.; Bogdanova, A.; Kraehenbuhl, J. P.; Pringault, E. Molecular Studies of the Intestinal Mucosal Barrier Physiopathology Using Cocultures of Epithelial and Immune Cells: A Technical Update. *Microbes Infect.* **2000**, *2*, 1119–1124.
20. Smith, M. W.; Thomas, N. W.; Jenkins, P. G.; Miller, N. G. A.; Cremaschi, D.; Porta, C. Selective Transport of Microparticles across Peyers Patch Follicle-Associated M-Cells from Mice and Rats. *Exp. Physiol.* **1995**, *80*, 735–743.
21. Florence, A. T. The Oral Absorption of Micro- and Nanoparticulates: Neither Exceptional Nor Unusual. *Pharm. Res.* **1997**, *14*, 259–266.
22. Florence, A. T. Nanoparticle Uptake by the Oral Route: Fulfilling Its Potential. *Drug Discovery Today Tech.* **2005**, *2*, 75–81.
23. Hariharan, S.; Bhardwaj, V.; Bala, I.; Sitterberg, J.; Bakowsky, U.; Ravi Kumar, M. N. V. Design of Estradiol Loaded PLGA Nanoparticulate Formulations: A Potential Oral Delivery System for Hormone Therapy. *Pharm. Res.* **2006**, *23*, 184–195.
24. Hillery, A. M.; Jani, P. U.; Florence, A. T. Comparative, Quantitative Study of Lymphoid and Nonlymphoid Uptake of 60 nm Polystyrene Particles. *J. Drug Targeting* **1994**, *2*, 151–156.
25. Hillyer, J. F.; Albrecht, R. M. Gastrointestinal Persorption and Tissue Distribution of Differently Sized Colloidal Gold Nanoparticles. *J. Pharm. Sci.* **2001**, *90*, 1927–1936.
26. Hodges, G. M.; Carr, E. A.; Hazzard, R. A.; Carr, K. E. Uptake and Translocation of Microparticles in Small-Intestine—Morphology and Quantification of Particle Distribution. *Dig. Dis. Sci.* **1995**, *40*, 967–975.
27. Jani, P.; Halbert, G. W.; Langridge, J.; Florence, A. T. The Uptake and Translocation of Latex Nanospheres and Microspheres after Oral Administration to Rats. *J. Pharm. Pharmacol.* **1989**, *41*, 809–812.
28. Jepson, M. A.; Clark, M. A.; Foster, N.; Mason, C. M.; Bennett, M. K.; Simmons, N. L.; Hirst, B. H. Targeting to Intestinal M Cells. *J. Anat.* **1996**, *189*, 507–516.
29. Panessa-Warren, B. J.; Warren, J. B.; Maye, M. M.; Van der Lelie, D.; Gang, O.; Wong, S. S.; Ghebrehiwet, B.; Tortora, G. T.; Misewich, J. A. Human Epithelial Cell Processing of Carbon and Gold Nanoparticles. *Int. J. Nanotechnol.* **2008**, *5*, 55–91.
30. Fabian, G. Persorption—The Way of Large Sized Corpuscle Particles *via* the Lymphatic System. *Lymphology* **1983**, *16*, 43–48.
31. Park, E. J.; Yi, J.; Chung, Y. H.; Ryu, D. Y.; Choi, J.; Park, K. Oxidative Stress and Apoptosis Induced by Titanium Dioxide Nanoparticles in Cultured BEAS-2B Cells. *Toxicol. Lett.* **2008**, *180*, 222–229.
32. Lin, W. S.; Xu, Y.; Huang, C. C.; Ma, Y. F.; Shannon, K. B.; Chen, D. R.; Huang, Y. W. Toxicity of Nano- And Micro-Sized ZnO Particles in Human Lung Epithelial Cells. *J. Nanopart. Res.* **2009**, *11*, 25–39.
33. Fischer, H. C.; Chan, W. C. W. Nanotoxicity: The Growing Need for *In Vivo* Study. *Curr. Opin. Biotechnol.* **2007**, *18*, 565–571.
34. Popielarski, S. R.; Pun, S. H.; Davis, M. E. A Nanoparticle-Based Model Delivery System To Guide the Rational Design of Gene Delivery to the Liver. 1. Synthesis and Characterization. *Bioconjugate Chem.* **2005**, *16*, 1063–1070.
35. Walter, E.; Kissel, T. Transepithelial Transport and Metabolism of Thyrotropin-Releasing-Hormone (TRH) in Monolayers of a Human Intestinal-Cell Line (Caco-2)—evidence for an Active-Transport Component. *Pharm. Res.* **1994**, *11*, 1575–1580.
36. Shukla, R.; Bansal, V.; Chaudhary, M.; Basu, A.; Bhonde,

R. R.; Sastry, M. Biocompatibility of Gold Nanoparticles and Their Endocytotic Fate Inside the Cellular Compartment: A Microscopic Overview. *Langmuir* **2005**, *21*, 10644–10654.
37. Garcia-Garcia, E.; Andrieux, K.; Gil, S.; Kim, H. R.; Le Doan, T.; Desmaele, D.; d'Angelo, J.; Taran, F.; Georgin, D.; Couvreur, P. *A Methodology To Study Intracellular Distribution of Nanoparticles in Brain Endothelial Cells*, 5th European Workshop on Particulate Systems; London, England, 2004, 310−314.
38. Jung, T.; Kamm, W.; Breitenbach, A.; Kaiserling, E.; Xiao, J. X.; Kissel, T. Biodegradable Nanoparticles for Oral Delivery of Peptides: Is There a Role for Polymers To Affect Mucosal Uptake? *Eur. J. Pharm. Biopharm.* **2000**, *50*, 147–160.
39. Olivier, V.; Duval, J. L.; Hindie, M.; Pouletaut, P.; Nagel, M. D. Comparative Particle-Induced Cytotoxicity toward Macrophages and Fibroblasts. *Cell Biol. Toxicol.* **2003**, *19*, 145–159.
40. Wyllie, A. H.; Kerr, J. F. R.; Currie, A. R. Cell Death: The Significance of Apoptosis. *Int. Rev. Cytol.* **1980**, *68*, 251–306.
41. Searle, J.; Kerr, J. F. R.; Bishop, C. J. Necrosis and Apoptosis—distinct Modes of Cell-Death with Fundamentally Different Significance. *Pathol. Annu.* **1982**, *17*, 229–259.
42. van Engelend, L. J. W.; Ramaekers, F. C. S.; Schutte, B.; Reutelingsperger, P. M. AnnexinV—Affinity Assay: A Review on an Apoptosis Detection System Based on Phosphatidylserine Exposure. *Cytometry* **1998**, *31*, 1–9.
43. Susin, S. A.; Zamzami, N.; Kroemer, G. The Cell Biology of Apoptosis: Evidence for the Implication of Mitochondria. *Apoptosis* **1996**, *1*, 231–242.
44. Riedl, s. J.; Shi, Y. Molecular Mechanisms of Caspase Regulation during Apoptosis. *Nat. Rev. Mol. Cell Biol.* **2004**, *5*, 897–907.
45. Hara, A.; Hibi, T.; Yoshioka, M.; Hayashi, A.; Toda, K.; Suzuki, T.; Kameda, Y.; Ueda, F.; Watanabe, M.; Tsuchiya, M. Quantitative-analysis of Intercellular Communication in Colon Cancer-Cells (Caco-2) by the Scrape-Loading Dye Transfer Assay. *Gastroenterol. Jpn.* **1992**, *27*, 560.
46. Jain, A. K.; Dubes, R. C. *Algorithms for Clustering Data*; Prentice Hall: Englewood Cliffs, NJ, 1988.
47. Lang, R; Lustig, M.; Francois, F.; Sellinger, M.; Plesken, Y. Apoptosis during Macrophage-Dependent Ocular Tissue Remodeling. *Development* **1994**, *120*, 3395–3403.
48. Reznikov, K.; Kolesnikova, L.; Pramanik, A.; Tan-no, K.; Gileva, I.; Yakovleva, T.; Rigler, R.; Terenius, L.; Bakalkin, G. Clustering of Apoptotic Cells *via* Bystander Killing by Peroxides. *FASEB J.* **2000**, *14*, 1754–1764.
49. Bojarski, C.; Weiske, J.; Schoneberg, T.; Schroder, W.; Mankertz, J.; Schulzke, J. D.; Florian, P.; Fromm, M.; Tauber, R.; Huber, O. The Specific Fates of Tight Junction Proteins in Apoptotic Epithelial Cells. *J. Cell Sci.* **2004**, *117*, 2097–2107.
50. Sayes, C. M.; Gobin, A. M.; Ausman, K. D.; Mendez, J.; West, J. L.; Colvin, V. L. Nano-C60 Cytotoxicity Is Due to Lipid Peroxidation. *Biomaterials* **2005**, *26*, 7587–7595.
51. Sun, T.; Xu, Z. Radical Scavenging Activities of α-Alanine C60 Adduct. *Bioorg. Med. Chem. Lett.* **2006**, *16*, 3731–3734.
52. Berger, T. M.; Polidori, M. C.; Dabbagh, A.; Evans, P. J.; Halliwell, B.; Morrow, J. D.; Roberts, L. J.; Frei, B. Antioxidant Activity of Vitamin C in Iron-Overloaded Human Plasma. *J. Biol. Chem.* **1997**, *272*, 15656–15660.
53. Xia, T.; Kovochich, M.; Brant, J.; Hotze, M.; Sempf, J.; Oberley, T.; Sioutas, C.; Yeh, J. I.; Wiesner, M. R.; Nel, A. E. Comparison of the Abilities of Ambient and Manufactured Nanoparticles To Induce Cellular Toxicity According to an Oxidative Stress Paradigm. *Nano Lett.* **2006**, *6*, 1794–1807.
54. Bach, F.; Hirschhorn, K. Lymphocyte Interaction: A Potential Histocompatibility Test *In Vitro*. *Science* **1964**, *143*, 813–814.
55. Brown, D. M.; Wilson, M. R.; MacNee, W.; Stone, V.; Donaldson, K. Size-Dependent Proinflammatory Effects of Ultrafine Polystyrene Particles: A Role for Surface Area and Oxidative Stress in the Enhanced Activity of Ultrafines. *Toxicol. Appl. Pharmacol.* **2001**, *175*, 191–199.
56. Wang, X. T.; McCullough, K. D.; Wang, X. J.; Carpenter, G.; Holbrook, N. J. Oxidative Stress-Induced Phospholipase C-1 Activation Enhances Cell Survival. *J. Biol. Chem.* **2001**, *276*, 28364–28371.
57. Davies, P. F.; Barbee, K. A.; Volin, M. V.; Robotewskyj, A.; Chen, J.; Joseph, L.; Griem, M. L.; Wernick, M. N.; Jacobs, E.; Polacek, D. C. Spatial Relationships in Early Signaling Events of Flow-Mediated Endothelial Mechanotransduction. *Annu. Rev. Physiol.* **1997**, *59*, 527–549.
58. Irani, K.; Xia, Y.; Zweier, J. L.; Sollott, S. J.; Der, C. J.; Fearon, E. R.; Sundaresan, M.; Finkel, T.; Goldschmidt-Clermont, P. J. Mitogenic Signaling Mediated by Oxidants in Ras-Transformed Fibroblasts. *Science* **1997**, *275*, 1649–1652.
59. Xue, M.; Hsieh, G.; Raymond-Stintz, M. A.; Pfeiffer, J.; Roberts, D.; Steinberg, S. L.; Oliver, J. M.; Prossnitz, E. R.; Lidke, D. S.; Wilson, B. S. Activated N-Formyl Peptide Receptor and High-Affinity IgE Receptor Occupy Common Domains for Signaling and Internalization. *Mol. Biol. Cell* **2007**, *18*, 1410–1420.
60. Wilson, B. S.; Steinberg, S. L.; Liederman, K.; Pfeiffer, J. R.; Surviladze, Z.; Zhang, J.; Samelson, L. E.; Yang, L.; Kotula, P. G.; Oliver, J. M. Markers for Detergent-Resistant Lipid Rafts Occupy Distinct and Dynamic Domains in Native Membranes. *Mol. Biol. Cell* **2004**, *15*, 2580–2592.
61. Zhang, J.; Leiderman, K.; Pfeiffer, J. R.; Wilson, B. S.; Oliver, J. M.; Steinberg, S. L. Characterizing the Topography of Membrane Receptors and Signaling Molecules from Spatial Patterns Obtained Using Nanometer-Scale Electron-Dense Probes and Electron Microscopy. *Micron* **2006**, *37*, 14–34.
62. Diggle, P. J.; Besag, J.; Gleaves, J. T. Statistical Analysis of Spatial Point Patterns by Means of Distance Methods. *Biometrics* **1976**, 659–667.